DOI: 10.1002/((please add manuscript number))

**Article type: Communication**

# Flexible All-Solid-State Supercapacitors with High Volumetric Capacitances Boosted by Solution Processable MXene and Electrochemically Exfoliated Graphene

*Hongyan Li, Yang Hou, Faxing Wang, Martin R. Lohe, Xiaodong Zhuang,* Li Niu* and Xinliang Feng**

H. Li, Dr. Y. Hou, F. Wang, Dr. M. R. Lohe, Dr. X. Zhuang and Prof. X. L. Feng
Department of Chemistry and Food Chemistry and Center for Advancing Electronics Dresden (cfaed), Technische Universität Dresden, 01062 Dresden, Germany
E-mail: xiaodong.zhuang@tu-dresden.de; xinliang.feng@tu-dresden.de

H. Li and Prof. L. Niu
State Key Laboratory of Electroanalytical Chemistry, c/o Engineering Laboratory for Modern Analytical Techniques, Changchun Institute of Applied Chemistry, Chinese Academy of Sciences, Changchun, 130022, Jilin, China.
E-mail: lniu@ciac.ac.cn

H. Li
University of Chinese Academy of Sciences, 100049 Beijing, China

Keywords: MXene, exfoliated graphene, all-solid-state supercapacitor, volumetric capacitance, flexible micro-supercapacitors

Flexible energy storage devices have shown broad application prospects in modern electronics, such as portable smart phone and outdoor wearable energy harvesting and storage systems.[1] So far, tremendous efforts have been made for the development of flexible energy storage devices, such as thin-film batteries, thin-film supercapacitors, on-chip micro-supercapacitors, cable-like supercapacitors and batteries, etc.[1b, 2] The great thing is that more and more proof-of-concept flexible energy storage devices have been built up through using new processing methods or nanotechnologies, such as self-assembly, printing, *in-situ* growth of active materials, etc.[3] Unfortunately, most of these devices suffer from scale-up fabrication or low performance in comparison with the conventional non-flexible devices, mostly due to the poor compatibility among active materials, electrolytes and substrates.[3c]All-solid-state supercapacitors (ASSSs), including

conventional sandwich-type solid state supercapacitors and on-chip micro-supercapacitors (MSCs), have emerged as new-generation energy storage devices for modern electronics due to their short-term energy storage, burst-mode power delivery and ultra-long cycling stability.[4] Despite of a lot of preliminary works dedicated to this field, the pursuit of flexible supercapacitors with high volumetric capacitances remains a great challenge.

Two-dimensional (2D) transition metal carbides (MXenes), which possess metallic conductivity and hydrophilic surface, have been rapidly recognized as a promising type of electrode materials for lithium-ion batteries, supercapacitors, and oxygen evolution reactions since the pioneering work of the supercapacitors based on 2D $Ti_3C_2T_x$ by Gogotsi and co-workers in 2011.[1b, 5] However, MXenes are not good candidates for large-area flexible thin-film fabrication due to their relatively small size (~200 nm). In order to overcome this shortcoming, non-active polymers, such as charged polydiallyldimethylammonium chloride or an electrically neutral polyvinyl alcohol, have been utilized to hybridize with MXene as film electrodes for supercapacitors.[6] Apparently, non-active polymer additives will lead to the device thickness increase and sacrifice the electrical conductivity of MXene, which thus reduce the specific capacitance of as-manufactured supercapacitors.

In this work, we demonstrate the solution processing of hybrid inks based on MXene nanosheets (also named as $Ti_3C_2T_x$, 0.2 mg $mL^{-1}$) and electrochemically exfoliated graphene (EG, 0.15 mg $mL^{-1}$) for the fabrication of flexible energy devices. The achieved flexible MSCs delivered a significant areal capacitance of up to 3.26 mF $cm^{-2}$ and volumetric capacitance of up to 33 F $cm^{-3}$ at 2 mV $s^{-1}$, which are among the ultrahigh performances of reported graphene-based MSCs (~ 2.3 mF $cm^{-2}$ and ~ 20 F $cm^{-3}$, Table S2 in Supporting Information). Moreover, thin film electrodes for flexible ASSSs (the thickness of film electrode is 2.5 μm) are demonstrated, exhibiting outstanding volumetric capacitances of up to 216 F $cm^{-3}$ at a current density of 0.1 A $cm^{-3}$, which is superior to

the state-of-the-art ASSSs based on graphene and other electrochemically active materials. In the hybrid electrodes, the small sized MXene between the graphene layers not only act as active material and ideal "buffer" for enhanced electrolyte shuttling, but also function as a conducting spacer which prevents the irreversible $\pi$–$\pi$ stacking between the graphene sheets.[7]

**Figure 1** illustrates the fabrication of ASSSs based on solution-processable EGMXx:y (where x:y = 1:3, 1:9, 3:1, and 9:1) hybrid inks. A graphite foil was first electrochemically exfoliated to produce the EG powder by using a home-made exfoliation system (Figure S1). The resultant EG powder can be readily dispersed in isopropanol (IPA) by sonication for 5 h, affording a stable solution-processable EG dispersion (0.15 mg $mL^{-1}$) (Figure 1a). On the other hand, pristine $Ti_3AlC_2$ was etched by HF to remove Al species, generating multilayered $Ti_3C_2T_x$ powder (MXene, where T represents terminal groups, e.g., O, OH, or F, and $x$ is the number of terminal groups). The multilayered $Ti_3C_2T_x$ was dispersed in water by sonication for 5 h and then centrifuged to obtain the supernatant-containing $Ti_3C_2T_x$ nanoflakes (0.2 mg $mL^{-1}$) (Figure 1b and Figure S2). Afterwards, the hybrid ink was prepared *via* ultrasonication of the EG/MXene mixture with the weight ratio of 1:3 to produce EGMX1:3 dispersion in IPA, which will be used as the typical example hereafter if not noted otherwise (Figure 1c). Notably, the EGMX1:3 dispersion can be stable for at least one week without visible agglomeration, which qualifies it as reliable ink for solution processing and thin film electrode fabrication (Figure S3). The colloidal states of EG dispersion in IPA, MXene dispersion in water, and EGMX1:3 dispersion in IPA were identified by the Tyndall scattering effect by passing a red laser beam through the solution (Figure 1a-c). Subsequently, two pieces of EGMX1:3 films were tailored into a size (2 cm× 1 cm) and PVA/$H_3PO_4$ gel electrolyte was drop casted onto one side of each film. Finally, PVA/$H_3PO_4$ soaked glass fiber membrane was sandwiched between the two film electrodes to produce an ASSS (Figure 1e). EGMXx:y thin film electrodes, where x:y

represents the weight ratio of EG to MXene, were also fabricated by assembly *via* vacuum-assisted filtration (VAF) for ASSSs (Figures 1d).

In order to inspect the morphology of EG, MXene and EGMX1:3, the transmission electron microscopy (TEM) and scanning electron microscopy (SEM) were employed. Flat feature with wrinkling and the average thickness of 1.8 nm for EG nanosheets were observed (Figure 2a and S4). The selected area electron diffraction (SAED, inset in Figure 2a) exhibits a typical six-fold symmetric diffraction pattern with stronger diffraction for the (1-210) plane than the (0-110) plane, indicating the high crystallinity of a typical bilayer graphene sheet.[8] MXene demonstrates a lamellar morphology, but with much smaller lateral size of ~200 nm in comparison with EG (lateral size ~ 1 μm, Figure 2b and S5).[5a, 9] The typical TEM and SEM images of EGMX1:3 film (thickness of 2.5 μm) disclose that the EG functions as mechanical skeleton between the MXene nanoflakes (Figure 2c-d and S6). In addition, EGMX1:3 film with MXene nanoflakes and EG nanosheets alternately stacked structure was identified (Figure 2c and inset cross-section SEM image), rendering the plenty of interlayer spacing which is beneficial for the electrolyte transportation.[10] The high angle annular dark field scanning TEM (HAADF-STEM) and elemental mapping images clearly revealed the homogeneous distributions of Ti, C, O, and F in the EGMX1:3 hybrid film (Figures S7-S11).

The electrochemical behavior of EGMXx:y based ASSSs were next investigated by cyclic voltammetry (CV) and galvanostatic charge/discharge (GCD) (Figure 3a and 3b). It is clear that the integral areas of CV and the capacitance value of GCD for EGMX1:3 based ASSS both present the maximum values compared with EG and MXene based ASSSs. When we increased the content of EG (3:1, 9:1 or pure EG) for the hybrid electrode, the relative larger sized of EG would aggregate and therefore hinder the ion transportation. Oppositely, when we decreased the content of EG (1:9 or pure MXene) for the hybrid electrode, the relative small sized of MXene would not have a strong mechanical skeleton

and unable provide a long-distance conductivity of the EG/MXene electrode. In this work, the weight ratio of EG:MX=1:3 was found as a suitable weight ratio for the construction of the ASSS electrode in comparison with EGMX3:1, EGMX9:1, EGMX1:9, MXene, EG (Figures S12 - S14). The volumetric capacitances were calculated and shown in Figure 3c and 3d. Among these devices, EGMX1:3 based ASSS delivered the capacitance of 184 F $cm^{-3}$ at 0.2 A $cm^{-3}$, which is superior to those of EGMX3:1 (49 F $cm^{-3}$), EGMX9:1 (54 F $cm^{-3}$), EGMX1:9 (33 F $cm^{-3}$), rGOMX1:3 (4 F $cm^{-3}$), MXene (4 F $cm^{-3}$), and EG (22 F $cm^{-3}$). The quasi-rectangular CV curves of the EGMX1:3 based ASSS were observed at the high scan rate of 200 mV $s^{-1}$, indicating a quasi-electrical double layer capacitive (EDLC) behavior (Figure 3e and 3f).[11] Based on the discharging behavior in GCD curves, the volumetric capacitances of EGMX1:3 based ASSS were determined to be 216, 184, 153, 130, and 110 F $cm^{-3}$ at current densities of 0.1, 0.2, 0.5, 1, and 2 A $cm^{-3}$, respectively. Upon further increase of the current densities from 4 to 12 A $cm^{-3}$, the GCD curves still remained triangular shape, revealing excellent charge/discharge performance and superior capacitive characteristics (Figure S15 - S16). Remarkably, 93% of the coulombic efficiency could be retained at high current density (up to 12 A $cm^{-3}$) (Figure 3g).

EGMX1:3 based ASSS showed the good cycle stability, with 97.8% and 85.2% of initial volumetric capacitance preserved after 500 and 2500 cycles, respectively (Figure 3h). In order to reveal the conductivity influence on the electrochemical performance, the electrochemical impedance spectroscopy was further measured (Figure S17). The smallest charge transport resistance $R_{ct}$ of EGMX1:3 (4.76 Ω) was observed in contrast to pristine EG (22.07 Ω) and MXene (42.79 Ω). This result suggests the most favorable electron transport pathway within the EGMX1:3 electrode with respect to the pristine EG or MXene electrode for ASSSs.[12]

Energy density and power density are critical parameters used to compare different types of energy storage systems. Significantly, EGMX1:3 film based ASSS delivered the high

volumetric energy density of 3.4 mWh $cm^{-3}$ at a power density of 200 mW $cm^{-3}$ and 1.4 mWh $cm^{-3}$ at a high power density of 1600 mW $cm^{-3}$ (Figure 3i), which are much higher than those of the state-of-the-art graphene-based ASSSs, e.g., about 1 mWh $cm^{-3}$ and 0.05 W $cm^{-3}$ for PEDOT-cellulose paper, 1 mWh $cm^{-3}$ and 0.03 W $cm^{-3}$ for graphene hydrogel, 0.61 mWh $cm^{-3}$ and 0.05 W $cm^{-3}$ for TiN-$Fe_2N$, 0.54 mWh $cm^{-3}$ and 0.4 W $cm^{-3}$ for VN/CNTs-SSCs, and 0.32 mWh $cm^{-3}$ and 0.05 W $cm^{-3}$ for G/PANI-paper (see Table S1 in Supporting Information). [13] The high electrochemical energy output of the EGMX1:3 based ASSS can be attributed to a synergistic effect between the EG and the MXene components: (i) EG/MXene electrode afforded plenty of large interlayer spacing and exhibited a large accessible area that allowed efficient ion adsorption and desorption; (ii) the graphene layers could function as a mechanical skeleton and further enhance the long-distance conductivity of the EG/MXene electrode.

Flexibility and variable working window are crucial for modern portable and wearable energy storage devices.[14] Therefore, the CV curves for EGMX1:3 based ASSS were chosen to study the aforementioned requirement. From Figure 4a and 4b, it shows almost the same capacitive behavior at different bending angles, displaying excellent flexibility and stability of the device. In addition, such flexible ASSS can be operated in different working voltage ranging from 0.0-0.8 V to 0.0-1.8 V with quasi-rectangular shape at a scan rate of 200 mV $s^{-1}$ (Figure 4c). Moreover, different working windows (1, 3, 4 in Figure 4d) and prolonged discharging time (2 in Figure 4d) could be achieved by the series-parallel connection of as-fabricated ASSSs. For instance, the operating voltage of three devices in series was ~ 3 times of a single device under the same current density; while the discharge time of two devices in parallel was ~ 2 times of a single device. As manifested in Figure 4e and 4f, a red LED was lit for 8 min by three ASSSs in series under the planar or winding state. All of these results demonstrated that the working potential window and energy storage capacity could be well tailored.

On-chip or in-plane MSCs have emerged as potential candidates to complement or even replace micro-batteries in various applications due to their safety, fast charge-discharge and silicon-compatible features.[1a, 12, 15] Thus, in-plane flexible MSC was fabricated by spray coating the solution-processable EGMX1:3 ink onto a PET substrate through a mask (Figure 5a). The finger and channel widths of the mask were each 1000 μm and the finger length and thickness of the mask were 2 cm and 1 μm, respectively. CV curves were obtained at different scan rates from 10 to 200 mV $s^{-1}$ with PVA/$H_3PO_4$ gel electrolyte on interdigital MSC (Figure 5b). Quasi-rectangular CV curves were observed at high scan rate of 200 mV $s^{-1}$, showing a nearly ideal EDLC behavior. The areal and volumetric capacitances of EGMX1:3 based MSC were calculated and summarized in Figure 5c. Remarkably, the fabricated EGMX1:3 based MSC presented a ultrahigh areal capacitance of 3.26 mF $cm^{-2}$ and a volumetric capacitance of 33 F $cm^{-3}$ at 5 mV $s^{-1}$, which are superior to the state-of-the-art graphene based MSCs, e.g., about 0.51 mF $cm^{-2}$ and 3.1 F $cm^{-3}$ for reduced GO, 2.32 mF $cm^{-2}$ and 3.05 F $cm^{-3}$ for laser reduced GO film, 0.087 mF $cm^{-2}$ and 17.9 F $cm^{-3}$ for GO thin film, 2.16 mF $cm^{-2}$ and 1.08 F $cm^{-3}$ for graphene/CNTCs, and 2 mF $cm^{-2}$ and 20 F $cm^{-3}$ for EG/PH1000 hybrid film (see Table S2 in Supporting Information).[12, 15a, 16] To evaluate the electrochemical stability of the fabricated flexible MSCs, the CV curves in alternating flat and bent states were measured at a scan rate of 200 mV $s^{-1}$ for 2500 cycles, maintaining 94.6% of their initial performance after 500 cycles and long term stability with 82% of capacitance retention after 2500 cycles (Figure 5d). Furthermore, the EGMX1:3 based MSC also exhibited excellent flexibility with different bending angle measurements (Figure S18).

In summary, we have demonstrated the MXene and EG based solution processable ink for constructing thin film electrodes of flexible all-solid-state supercapacitors and in-plane micro-supercapacitors. Significantly, the EGMX1:3 based flexible MSC delivered a significant areal capacitance and volumetric capacitance as high as 3.26 mF $cm^{-2}$ and 33 F

$cm^{-3}$ at 5 mV $s^{-1}$, respectively, which are superior to those of the state-of-the-art graphene based MSCs. Moreover, profiting from the plenty of large interlayer spacing and good conductivity of EGMX1:3 thin film, the fabricated ASSS device exhibited outstanding volumetric capacitance of up to 216 F $cm^{-3}$ at 0.1 A $cm^{-3}$. Thereby the established ASSSs and MSCs based on solution processable hybrid inks of MXene/EG may pave the way for the future development of scalable high-performance portable and micro-sized integrated energy storage devices.

**Supporting Information**

Supporting Information is available from the Wiley Online Library or from the author.

**Acknowledgements**

This work was financially supported by ERC Grant on 2DMATER and EU Graphene Flagship. The authors thank Bin Cai, Yingjuan Sun and Lifang Gao for part of characterizations and discussion. H. Li acknowledges the PhD abroad scholarship from University of Chinese Academy of Sciences.

Received: ((will be filled in by the editorial staff))
Revised: ((will be filled in by the editorial staff))
Published online: ((will be filled in by the editorial staff))

[1] a) P. Huang, C. Lethien, S. Pinaud, K. Brousse, R. Laloo, V. Turq, M. Respaud, A. Demortière, B. Daffos, P. L. Taberna, B. Chaudret, Y. Gogotsi, P. Simon, *Science* **2016**, *351*, 691; b) J. Chmiola, C. Largeot, P. L. Taberna, P. Simon, Y. Gogotsi, *Science* **2010**, *328*, 480; c) L. Liu, Y. Yu, C. Yan, K. Li, Z. Zheng, *Nat. Commun.* **2015**, *6*, 7260. d) Y. Zhu, S. Murali, M. D. Stoller, K. J. Ganesh, W. Cai, P. J. Ferreira, A. Pirkle, R. M. Wallace, K. A. Cychosz, M. Thommes, D. Su, E. A. Stach, R. S. Ruoff, *Science* **2011**, *332*, 1537; e) B. Zheng, M. Shun, J. Zhao, C. Kefa, J. Chen, K. Ostrikov, *Chem. Soc. Rev* **2015**, *44*, 2108.

[2] a) G. Nystrom, A. Marais, E. Karabulut, L. Wagberg, Y. Cui, M. M. Hamedi, *Nat. Commun.* **2015**, *6*, 7259. b) L. Kou, T. Huang, B. Zheng, Y. Han, X. Zhao, K. Gopalsamy, H. Sun, C. Gao, *Nat. Commun.* **2014**, *5*, 3754.

[3] a) S. Liu, P. Gordiichuk, Z. S. Wu, Z. Liu, W. Wei, M. Wagner, N. Mohamed-Noriega, D. Wu, Y. Mai, A. Herrmann, K. Müllen, X. Feng, *Nat. Commun.* **2015**, *6*, 8817. b) Z. S. Wu, K. Parvez, S. Li, S. Yang, Z. Liu, S. Liu, X. Feng, K. Müllen, *Adv. Mater.* **2015**, *27*, 4054; c) Z. Yang, J. Ren, Z. Zhang, X. Chen, G. Guan, L. Qiu, Y. Zhang, H. Peng, *Chem. Rev.* **2015**, *115*, 5159.

[4] a) C. Hao, B. Yang, F. Wen, J. Xiang, L. Li, W. Wang, Z. Zeng, B. Xu, Z. Zhao, Z. Liu, Y. Tian, *Adv. Mater.* **2016**, *28*, 3194; b) M. F. El-Kady, R. B. Kaner, *Nat. Commun.* **2013**, *4*, 1475. c) X. Yang, C. Cheng, Y. Wang, L. Qiu, D. Li, *Science* **2013**, *341*, 534; d) Y. Gogotsi, P. Simon, *Science* **2011**, *334*, 917.

[5] a) M. Naguib, M. Kurtoglu, V. Presser, J. Lu, J. Niu, M. Heon, L. Hultman, Y. Gogotsi, M. W. Barsoum, *Adv. Mater.* **2011**, *23*, 4248; b) T. Ma, J. Cao, M. Jaroniec, S. Qiao, *Angew. Chem. Int. Ed.* **2016**, *55*, 1138. c) X. Wang, S. Kajiyama, H. Iinuma, E. Hosono, S. Oro, I. Moriguchi, M. Okubo, A. Yamada, *Nat. Commun.* **2015**, *6*, 6544.

[6] Z. Ling, C. E. Ren, M. Zhao, J. Yang, J. Giammarco, J. Qiu, M. W. Barsoum, Y. Gogotsi, *Proc. Natl. Acad. Sci. U S A/PNAS.* **2014**, *111*, 16676.

[7] a) M. Q. Zhao, C. E. Ren, Z. Ling, M. R. Lukatskaya, C. Zhang, K. L. Van Aken, M. W. Barsoum, Y. Gogotsi, *Adv. Mater.* **2015**, *27*, 339; b) C. Cheng, G. Jiang, C. J. Garvey, Y. Wang, P. Simon, J. Z. Liu, D. Li, *Science Advances* **2016**, *2*, e1501272; c) B. Mi, *Science* **2014**, *343*, 740.

[8] a) K. Parvez, Z. S. Wu, R. Li, X. Liu, R. Graf, X. Feng, K. Müllen, *J. Am. Chem. Soc.* **2014**, *136*, 6083. b) S. Yang, S. Bruller, Z. S. Wu, Z. Liu, K. Parvez, R. Dong, F. Richard, P. Samori, X. Feng, K. Müllen, *J. Am. Chem. Soc.* **2015**, *137*, 13927.

[9] M. Ghidiu, M. R. Lukatskaya, M. Q. Zhao, Y. Gogotsi, M. W. Barsoum, *Nature* **2014**, *516*, 78.

[10] G. Liu, W. Jin, N. Xu, *Chem. Soc. Rev.*, **2015**, *44*, 5016.

[11] Z. S. Wu, Z. Liu, K. Parvez, X. Feng, K. Müllen, *Adv. Mater.***2015**, *27*, 3669.

[12] Z. S. Wu, K. Parvez, X. Feng, K. Müllen, *Nat. Commun.* **2013**, *4*, 2487.

[13] a) B. Anothumakkool, R. Soni, S. N. Bhangea, S. Kurungot, *Energy Environ. Sci.*, **2015**, *8*, 1339; b) Y. Xu, Z. Lin, X. Huang, Y. Liu, Y. Huang, X. Duan, *ACS Nano* **2013**, *7*, 4042; c) C. Zhu, P. Yang, D. Chao, X. Wang, X. Zhang, S. Chen, B. K. Tay, H. Huang, H. Zhang, W. Mai, H. J. Fan, *Adv. Mater.* **2015**, *27*, 4566; d) X. Xiao, X. Peng, H. Jin, T. Li, C. Zhang, B. Gao, B. Hu, K. Huo, J. Zhou, *Adv. Mater.* **2013**, *25*, 5091; e) G. Sun, X. Zhang, R. Lin, J. Yang, H. Zhang, P. Chen, *Angew. Chem. Int. Ed.*

**2015**, *54*, 4651; f) B. Yao, L. Yuan, X. Xiao, J. Zhang, Y. Qi, J. Zhou, J. Zhou, B. Hu, W. Chen, *Nano Energy* **2013**, *2*, 1071; g) W. Zilong, Z. Zhu, J. Qiu, S. Yang, *J. Mater. Chem. C* **2014**, *2*, 1331; h) X. Lu, M. Yu, G. Wang, T. Zhai, S. Xie, Y. Ling, Y. Tong, Y. Li, *Adv. Mater.* **2013**, *25*, 267; i) L. Yuan, X. Lu, X. Xiao, T. Zhai, J. Dai, F. Zhang, B. Hu, X. Wang, L. Gong, J. Chen, *ACS Nano* **2011**, *6*, 656; j) Y. Kang, H. Chung, C. Han, W. Kim, *Nanotechnology* **2012**, *23*, 065401.

[14] L. Zheng, Z. Wang, M. Zhang, C. Yu, G. Wang, Y. Dong, S. Liu, Y. Wang, J. Qiu, *Adv. Funct. Mater*. **2016**, *26*, 111.

[15] a) Z. Liu, Z. Wu, S. Yang, R. Dong, X. Feng, K. Müllen, *Adv. Mater.* **2016**, *28*, 2217; b) R. Li, R. Peng, K. Kihm, S. Bai, D. Bridges, U. Tumuluri, Z. Wu, T. Zhang, G. Compagnini, Z. Feng, A. Hu, *Energy Environ. Sci.*, **2016**, *9*, 1458.

[16] a) W. Gao, N. Singh, L. Song, Z. Liu, A. L. M. Reddy, L. Ci, R. Vajtai, Q. Zhang, B. Wei, P. M. Ajayan, *Nat. Nanotechnol.* **2011**, 6, 496.; b) M. F. El-Kady, R. B. Kaner, *Nat. Commun.* **2013**, 4, 1475.

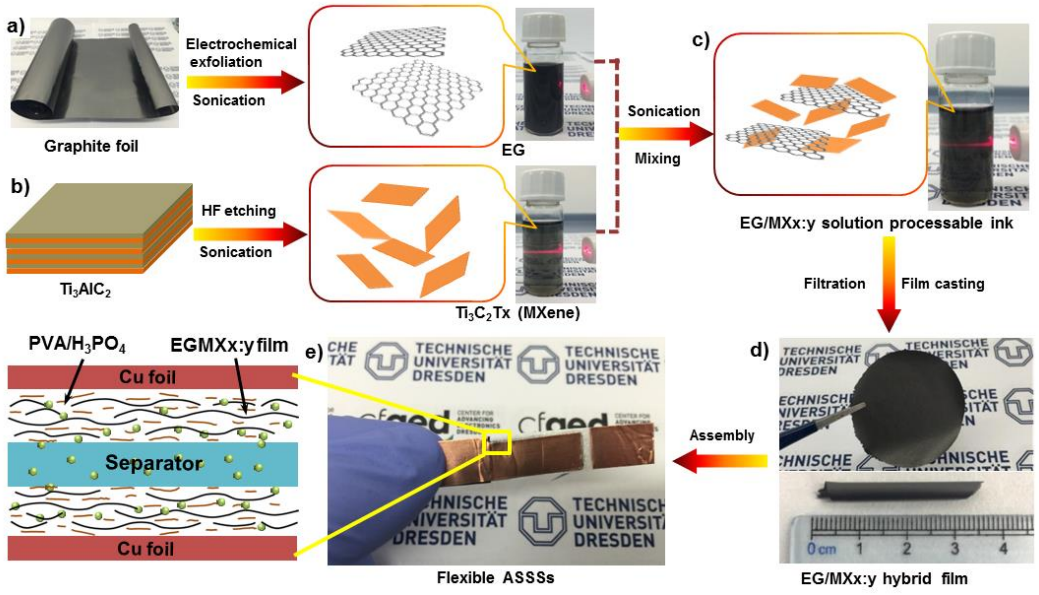


**Figure 1.** Materials preparation and devices fabrication. a) Schematic description of electrochemical exfoliation graphene and stable graphene-IPA dispersion. b) Schematic description of MXene ($Ti_3C_2T_x$) nanosheets and the stable MXene-water dispersion. c) Illustration of the fabrication process of EGMX1:3 nanohybrid dispersion. Note: The digital photographs of a), b), and c) show the Tyndall scattering effect in a colloidal solution of EG, MXene, and EGMX1:3 nanohybrid composite,

respectively. d) and e) The digital photographs of flexible and freestanding EGMX1:3 film and corresponding assembly of the ASSS.

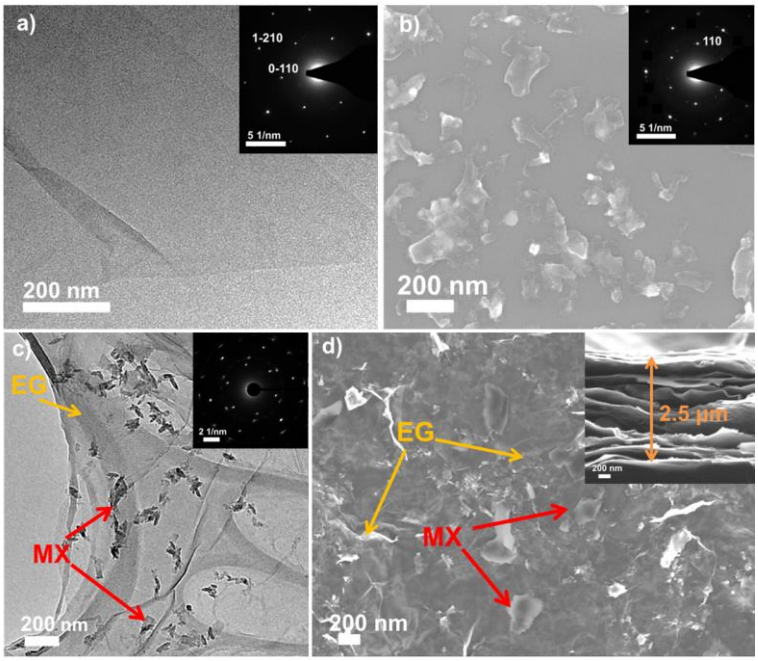


**Figure 2.** Microcosmic morphology of EG, MXene and EGMX1:3 hybrid film. a and c) Typical TEM images of EG and EGMX1:3 nanohybrid. b and d) Field emission SEM images of MXene and EGMX1:3 hybrid film. The insets in a), b) and c) are selected area electron diffraction (SAED) patterns of EG, MXene, and EGMX1:3, respectively; the inset in d) is the cross-section SEM image of EGMX1:3 film.

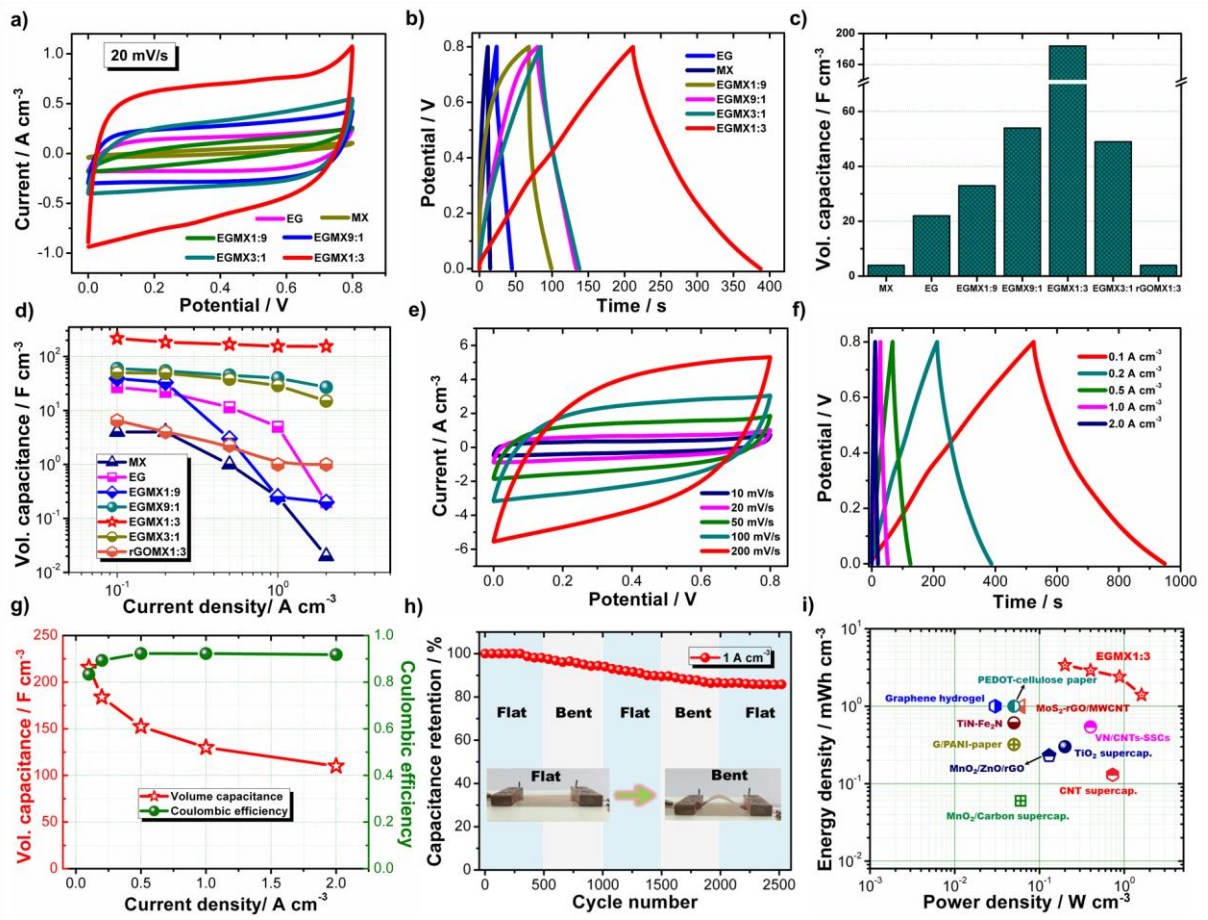


**Figure 3.** Electrochemical performance of the fabricated ASSSs. a) Comparison of CV curves of ASSSs based on EG, MXene, and EGMXx:y (where x:y = 1:3, 3:1, 1:9, and 9:1) at a scan rate of 20 mV $s^{-1}$. b) Comparison of galvanostatic charge/discharge (GCD) curves of ASSSs based on EG, MXene, and EGMXx:y at a current density of 0.2 A $cm^{-3}$. c) Volumetric capacitances of ASSSs based on EG, MXene, EGMXx:y and rGOMX1:3 at 0.2 A $cm^{-3}$. d) Volumetric capacitances of ASSSs based on EG, MXene, EGMXx:y, and rGOMX1:3 at different current densities. e) CV curves of the EGMX1:3 based ASSS recorded at different scan rates of 10, 20, 50, 100, and 200 mV $s^{-1}$. f) GCD curves of EGMX1:3 based ASSS recorded at different current densities of 0.1, 0.2, 0.5, 1, and 2A $cm^{-3}$. g) Correlations between volumtric capacitance and coulombic efficiency with different current densities. h) EGMX1:3 based ASSS capacitance retention after 2500 cycles at a current density of 1 A $cm^{-3}$. i) Ragone plots for EGMX1:3 based ASSS in comparison with several reported supercapacitors.

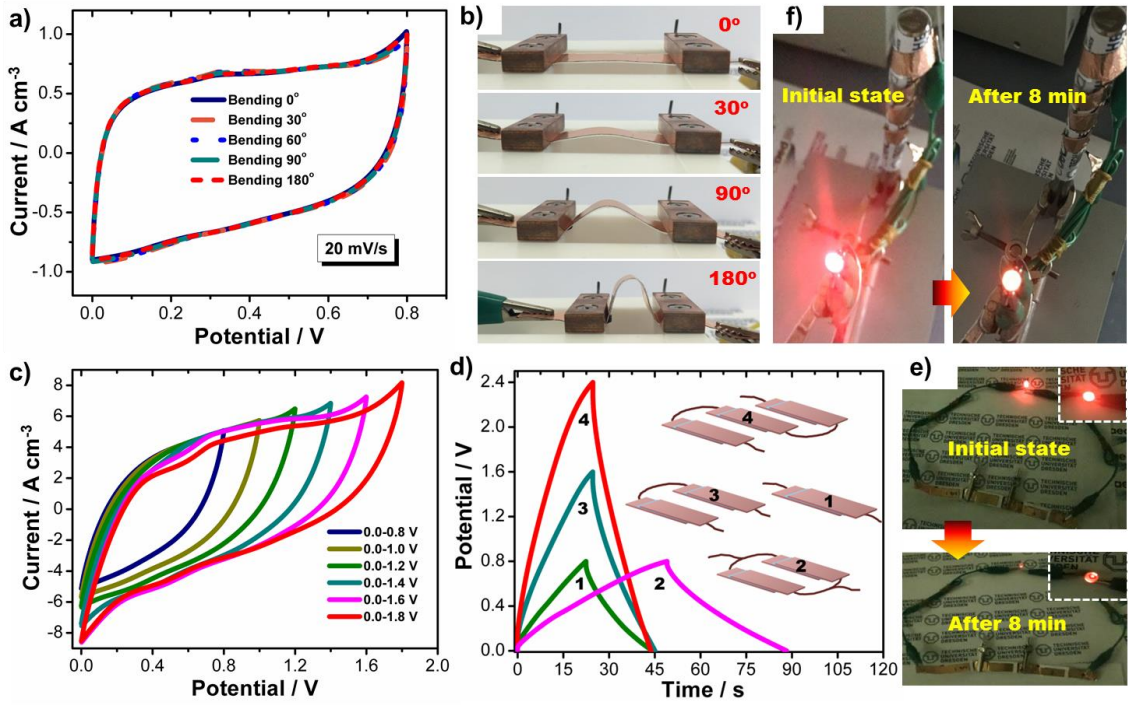


**Figure 4.** Flexibility and voltage window control of the fabricated ASSSs. a) CV curves of EGMX1:3 based ASSSs bended at different angles of 30°, 90° and 180° at 20 mV $s^{-1}$. b) Digital photographs of EGMX1:3 based ASSS bended at different angles. c) CV curves of the ASSS devices in different scan potential windows at 200 mV $s^{-1}$. d) GCD curves of single ASSS, two ASSSs in parallel, and two and three ASSSs connected in series; the insets depict cartoons of the ASSSs connected in series and in parallel. e) and f) Optical images of a LED powered using the three tandem ASSSs in winding and in plane. The inset shows an LED illuminated for more than 8 min by three tandem ASSS devices.

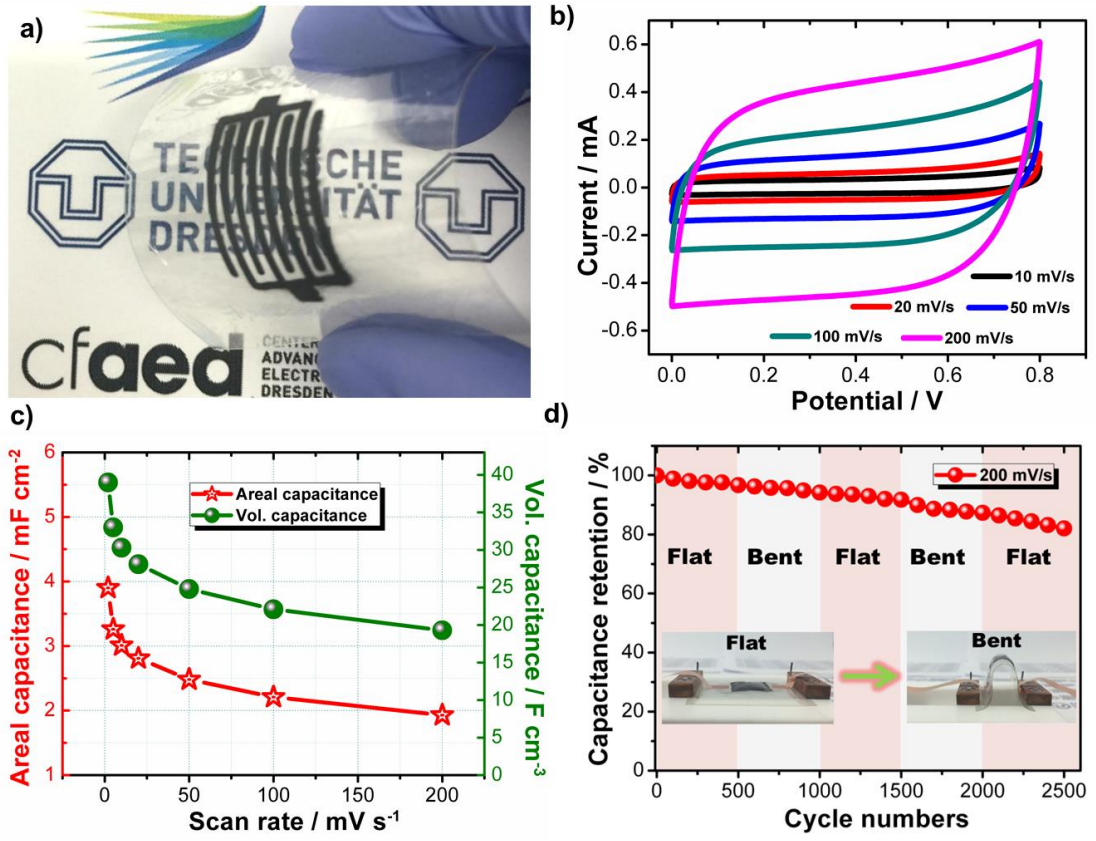


**Figure 5.** Electrochemical performance and flexibility studies of the fabricated MSCs. **(**a) Photograph of the flexible in-plane MSC based on EGMX1:3 hybrid ink on a PET substrate. (b) CV curves of MSC based on EGMX1:3 at different scan rates of 10, 20, 50, 100, and 200 mV $s^{-1}$. (c) Areal capacitance and volumetric capacitance of MSC based on EGMX1:3 nanohybrid at different scan rates. (d) The capacitance retention in the alternative flat and bent configurations after 2500 cycles at a scan rate of 200 mV $s^{-1}$. The inset shows the photographs of the micro-device in the flat and bent configurations.